Solar Energy Materials & Solar Cells 230 (2021) 111238

Contents lists available at ScienceDirect

Solar Energy Materials and Solar Cells

journal homepage: www.elsevier.com/locate/solmat

Phase separation of VO_2 and SiO_2 on SiO_2-Coated float glass yields robust thermochromic coating with unrivalled optical properties

Cindy P.K. Yeung [a,b], Roberto Habets [a,b], Luc Leufkens [a,b], Fallon Colberts [c], Kathleen Stout [c], Marcel Verheijen [d,e], Zeger Vroon [a,b,c], Daniel Mann [a,b,*], Pascal Buskens [a,b,f,**]

[a] The Netherlands Organisation for Applied Scientific Research (TNO), High Tech Campus 25, 5656AE, Eindhoven, the Netherlands
[b] Brightlands Materials Center, Urmonderbaan 22, 6167RD, Geleen, the Netherlands
[c] Zuyd University of Applied Sciences, Nieuw Eyckholt 300, 6400AN, Heerlen, the Netherlands
[d] Department of Applied Physics, Eindhoven University of Technology, 5600MB, Eindhoven, the Netherlands
[e] Eurofins Materials Science, 5656AE, Eindhoven, the Netherlands
[f] Hasselt University (UHasselt), Institute for Materials Research (IMO), DESINe Group, Martelarenlaan 42, 3500, Hasselt, Belgium

ARTICLE INFO

Keywords:
Thermochromic
Coating
Sol-gel
Vanadium dioxide
Silica
Smart window
Energy-efficiency
Building energy simulations

ABSTRACT

Vanadium dioxide displays thermochromic properties based on its structural phase transition from monoclinic VO_2 (M) to rutile VO_2 (R) and *vice versa*, and the accompanying reversible metal-insulator transition. We developed a single layer coating comprising VO_2 (M) and SiO_2. We applied the coating from an alcoholic solution comprising vanadium(IV) oxalate complex and pre-oligomerized tetra ethoxy silane to SiO_2-coated float glass using dip coating, and thermally annealed the dried xerocoat in a two-step process. The addition of SiO_2 as coating matrix resulted in non-scattering coatings with low surface roughness and random distribution of VO_2 nanodomains ($\leq$200 nm). Furthermore, the formation of the coating, comprising a phase separation yielding SiO_2 and VO_2 nanodomains during the thermal anneal, was studied in detail. The coating displays unrivalled optical properties, combining high visible light transmission $T_{vis} > 60\%$ and large solar modulation $\Delta T_{sol} \geq 10\%$. When applied in insulating glass units, the coating has a positive impact on energy savings for heating and cooling of buildings in intermediate climates, which we demonstrated through building energy simulations. For a typical house in the Netherlands, energy savings up to 24% were obtained. In addition, we demonstrate a coating stability comparable to current energy-efficient window coatings during processing into and in insulating glass units through (accelerated) life time tests.

1. Introduction

Thermochromic coatings are of interest for application in smart windows since they change their light transmission at a critical switching temperature T_0 [1–3]. The thermochromic material that is most promising for use in window coatings is monoclinic vanadium dioxide – VO_2 (M) [3–5]. VO_2 (M) undergoes a structural phase transition to rutile VO_2 (R) at $T_0 = 68$ °C, which is reversible and accompanied by a metal-insulator transition (MIT). Dopants, such as W, can reduce T_0 to values between 15 °C and 30 °C, which is ideal for smart windows. The MIT does not only cause a change in the electrical but also in the optical properties of the coating [3]. When switching from VO_2 (M) to VO_2 (R), the transmission of solar infrared (IR) light decreases. This leads to a reduction in solar heat gain at high outside temperatures, keeps buildings cooler in summer and reduces the energy consumption and costs for the use of air-conditioning systems. The benefits of using VO_2 in window coatings are that the switch in optical properties occurs mainly in the solar IR region and is therefore largely invisible [6], that the change in light transmission between the high temperature and low temperature phase can be tuned, e.g. by varying coating thickness [3] or composition [7], and that the switching temperature can be adjusted by addition of dopants [8]. The switching temperature is defined either as the temperature at start of the structural phase transition (T_0; thermodynamically relevant temperature) [9], or as the temperature of the heat flow optimum (T_{switch}; commonly reported in application oriented publications) [3]. Many studies have been published investigating VO_2 in

* Corresponding author. The Netherlands Organisation for Applied Scientific Research (TNO), High Tech Campus 25, 5656AE, Eindhoven, the Netherlands.
** Corresponding author. The Netherlands Organisation for Applied Scientific Research (TNO), High Tech Campus 25, 5656AE, Eindhoven, the Netherlands.
E-mail addresses: Daniel.Mann@tno.nl (D. Mann), Pascal.Buskens@tno.nl (P. Buskens).

https://doi.org/10.1016/j.solmat.2021.111238
Received 7 May 2021; Received in revised form 9 June 2021; Accepted 11 June 2021
Available online 21 June 2021

single [7,10,11] or multi-layer coatings [12,13], nanoporous [14–17] or nanocomposite single layers [7,16–19], incorporated in multilayer antireflective coating stacks [20–23], or as pigment material in nanocomposite polymer films [24–27]. Major goal of these studies was to optimize the optical properties of VO_2 by combining high visible transmission (T_{vis}) with a high solar modulation (ΔT_{sol}), where

$$T_{vis,sol} = \frac{\int \varphi_{vis,sol}(\lambda) T(\lambda) d\lambda}{\int \varphi_{vis,sol}(\lambda) d\lambda} \quad (1)$$

$$\Delta T_{sol} = T_{sol,cold} - T_{sol,hot} \quad (2)$$

with $T(\lambda)$ as the transmittance at wavelength λ, $\Phi_{vis}(\lambda)$ as the photopic spectral sensitivity of human vision, and $\Phi_{sol}(\lambda)$ as the AM 1.5 solar irradiance spectrum. Nevertheless, due to various drawbacks of the different types of coatings, no coating suitable for industrial scale implementation in smart windows has been reported to date. Single and multilayer coatings of pure VO_2 suffer from the non-linear change of refractive index (n) upon phase transition [23]. For such coatings the refractive index in wavelength regions below 2 μm is lower for the high temperature rutile phase VO_2 (R) than the low temperature monoclinic phase VO_2 (M). Only in high wavelength regions above 2 μm does the refractive index increase while changing from VO_2 (M) to VO_2 (R). This leads to reduced reflection at high temperatures, and therefore increased transmission especially in the wavelength region between 500 and 900 nm [23]. Therefore, even for thick coatings, which display low T_{vis}, only moderate values for ΔT_{sol} are reached [3]. These issues can be circumvented by e.g. including the VO_2 layer in an antireflective coating stack. Here, by carefully adjusting the refractive index of all layers, high ΔT_{sol} values of up to 21.8% can be reached at T_{vis} ranging from 45 to 55% [20–23]. For commercial application these systems are less relevant due to their complexity with multiple coating layers, which leads to high production costs. Another possibility to tune the refractive index of the VO_2 layer is by creating nanoporous or nanocomposite coatings. The introduction of nanometer sized air pockets [14–17] or low refractive index material as matrix for VO_2 domains [7,16–19] can lead to a better balance between T_{vis} and ΔT_{sol}. Most of the methods to prepare these types of coatings, e.g. via hydrothermal growth of coatings on glass [14], via freeze-drying [15] or coatings comprising porous or core-shell nanoparticles [16,17], are not feasible on commercial scale. Other methods that are applicable for large scale production only show large ΔT_{sol} at low $T_{vis} < 50\%$ [7,18,19]. The only systems reported to date that combine high $T_{vis} > 60\%$ with large $\Delta T_{sol} \geq 10\%$ in processes viable for large scale production are nanocomposite polymer films [24–27], which can be used as interlayers in laminated glass. The introduction of VO_2 nanopigments in several micrometer thick polymer films can lead to a combination of high T_{vis} and large ΔT_{sol} values. However, most of these nanocomposite films exhibit a broad hysteresis and transition gradient [24–27], which negatively affect the energy savings potential of smart windows [28]. Recently, Ciu et al. [3] reviewed the developments on VO_2-based thermochromic coatings and films, and concluded that for application in smart windows it is desired to combine high T_{vis} (>60%) with high ΔT_{sol} (≥10%) which has not yet been achieved with single-layer thermochromic coatings. One of the most promising approaches using an industrially relevant technique was reported by Schläfer et al. [7]. Here composite coatings, integrating small VO_2 domains in an SiO_2 matrix via a sol-gel coating technique, were investigated. They reported an optimized balance between T_{vis} and ΔT_{sol} and showed via theoretical calculations on different compositions and optical constants the potential of these composite coatings. Even though the theoretical calculations projected that it should be possible to combine high $\Delta T_{sol} \geq 10\%$ with $T_{vis} > 60\%$ using this system, only $T_{vis} < 53\%$ at $\Delta T_{sol} \geq 10\%$ was achieved in composite coatings.

To progress the development of thermochromic VO_2 coatings from a promising concept to successful market introduction in energy-efficient glazing, it is important to develop a robust coating that combines high $T_{vis} > 60\%$ with high $\Delta T_{sol} \geq 10\%$ in a production process that is feasible at commercial scale. Furthermore, the coating has to be stable under processing conditions for integration of coated glass plates in an insulating glass unit (IGU), and for more than 10 years within the final IGU installed in a building. We addressed all these challenges and report the first robust nanocomposite single layer VO_2 coating combining high $T_{vis} > 60\%$ with large $\Delta T_{sol} \geq 10\%$ applied in a cost efficient and commercially feasible process. We developed a single layer coating comprising VO_2 (M) and SiO_2. We applied the coating from an alcoholic solution comprising vanadium(IV) oxalate complex and pre-oligomerized tetra ethoxy silane to SiO_2-coated float glass using dip coating, and thermally annealed the xerocoat in a two-step process. The formation of the coating, comprising a phase separation during the thermal anneal yielding SiO_2 and VO_2 nanodomains, was studied in detail. We investigated the influence of the VO_2 (M) concentration and thickness of the nanocomposite coating on T_{vis} and ΔT_{sol} of the coated glass. Furthermore, we analyzed the stability of a single side coated glass plate for common processing conditions of glass plates into an IGU and we performed accelerated lifetime tests according to standards for IGUs coated on the inside of the outer glass pane (layer 2, Fig. 1). Additionally, we studied the energy savings potential of our high performance coatings in an average Dutch building using building energy simulations.

2. Materials and methods

2.1. Materials

Vanadium(V) oxide (V_2O_5, 99.6%), oxalic acid (98%) and 2-propanol (99.8%) were purchased from Sigma-Aldrich. Acetic acid (99.9%) was purchased from Alfa Aesar. Tetraethoxysilane (TEOS, 98%) was purchased from Acros Organics. Nitric acid (65%) was purchased from Fisher Chemicals. Nitrogen gas (N_2, HiQ 6.0) was purchased from Linde Gas. All chemical were used as received without further purification. Vanadyl oxalate solution and silica sol were prepared via previously reported procedures [9]. As glass substrates 10 × 10 cm^2 Pilkington Optiwhite^{tm} glass plates of 4 mm thickness were used. Prior to application of the thermochromic coating the glass substrate was cleaned and a silica barrier coating was applied according to a previously reported procedure [9]. All coating experiments were performed at a relative humidity below 35% and a temperature between 19 °C and 25 °C.

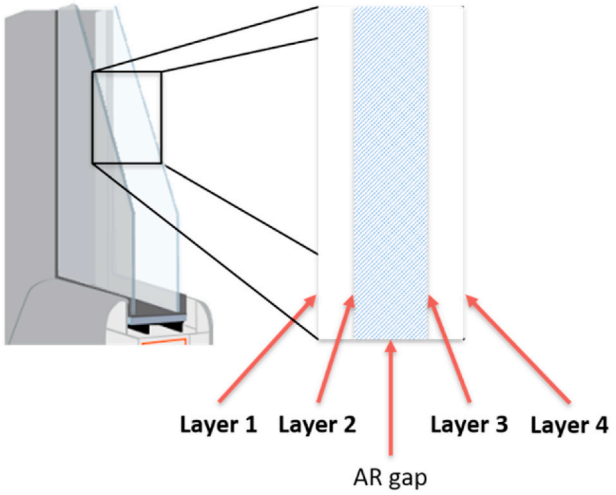

Fig. 1. IGU with typical labeling of the individual glass surfaces. Layer 1 is in contact with the outside environment and layer 4 with the inside environment. Our thermochromic coating is applied on layer 2.

2.2. Preparation of thermochromic coatings

One side of the barrier coated glass substrate was masked using d-c-fix® self-adhesive foil. Subsequently, the thermochromic coating was applied to the non-covered, non-tin side using dip coating. The applied liquid coating formulation consisted of a mixture of vanadyl oxalate solution and silica sol at an appropriate ratio of SiO_2 to VO_2 to reach the desired composition (Table 1). The xerogel coating was applied to the glass substrates at withdrawal speeds in the range of 1.0–5.0 mm s^{-1} to achieve the desired thickness. After drying for 5 min under ambient conditions, the adhesive foil was removed. The non-coated side was then placed onto a 6 inch silica wafer, and annealed in a Jipelec Jetfirst PV Rapid Thermal Processor, with the coated side facing the IR radiators. The coated glass plates were first heated to 270 °C in air for 480 s, and subsequently in N_2 at 450 °C for 30 s.

2.3. Building energy simulations

Building energy simulations have been performed using Energy Plus version 9.2.0 [29]. The selected simulation period was one year with data points gathered monthly. For a typical Dutch building (Fig. S1) one half of a three story duplex house was chosen with a floor area of 5 × 10 m^2 and a ceiling height of 2.6 m (Fig. 2). With a 45° roof pitch starting at the second floor level, a total living space of 130 m^2 was obtained according to standard definitions. All walls were designed facing one cardinal direction with the western wall not in contact to the outside environment. In agreement with typical window surface values for duplex houses in the Netherlands, we selected a total window surface of 35 m^2. The outer walls were designed according to Dutch regulations to reach a thermal insulation value (*Rc*-value) of at least 4.5 m^2 K W^{-1}. For detailed description of wall material and built up see supporting information (Fig. S2, Tables S1 and S2). Illuminance level and lighting loads were adjusted to reach average annual energy consumption values for lighting for a 4 person household in the Netherlands. All other parameters were used as reported in our previous building energy simulation study [30].

3. Results and discussion

3.1. Preparation of thermochromic VO_2:SiO_2 coatings with varying composition and thickness

To study the influence of composition and coating thickness on T_{vis} and ΔT_{sol}, we prepared coatings with three different VO_2:SiO_2 ratios and three different thicknesses. As a reference we prepared a pure VO_2 coating of approximately 100 nm thickness (Fig. 3d, Table 1). For varying composition we selected mixtures resulting in coatings with 40, 50 and 70% v/v VO_2 (Fig. 3a–c, Table 1). Therefore, we prepared mixtures of vanadyl oxalate solution and silica sol in appropriate molar ratios to lead to the desired composition, assuming standard densities for VO_2 and SiO_2 of 4.57 g cm^{-3} and 1.50 g cm^{-3}, respectively. For all coatings with varying composition the overall solid content in the coating formulation and the withdrawal speed of the dip coater were kept constant to lead to coating thicknesses around 100 nm (Table 1). To investigate the influence of the coating thickness on the optical properties we selected a 50% v/v composition. By adjusting the withdrawal speed of the dip coater at a constant solid content in the coating formulation, we prepared coatings with thickness of 47, 96 and 140 nm (Fig. 3e–g, Table 1). All coatings were prepared on Pilkington Optiwhite^{tm} soda-lime glass with a pre-deposited silica barrier layer and were subjected to a 2-step curing procedure after dip coating. Here it was especially important to control the temperature and atmosphere during the curing procedures. The first curing step at 270 °C under air was needed to remove oxalate ligands and excess oxalic acid, and the second curing step under inert gas at 450 °C was required for the crystallization of VO_2 (TGA see supporting information, Fig. S3). The temperature for the crystallization step was hereby limited by the softening temperature of float glass of 470 °C. A qualitative analysis of the VO_2:SiO_2 coatings **1–3** showed optical homogeneity and no scattering of visible light. All coatings show low haze and glare values of < 1% with almost no reflection haze (Fig. S4). Furthermore, we qualitatively observed an increased tinting level with increasing VO_2 content and/or layer thickness, with the highest tinted coating **3** reaching almost the same tinting level as pure VO_2 (Fig. 3). A quantitative investigation of the optical properties including switching behavior is presented in section 3.3.

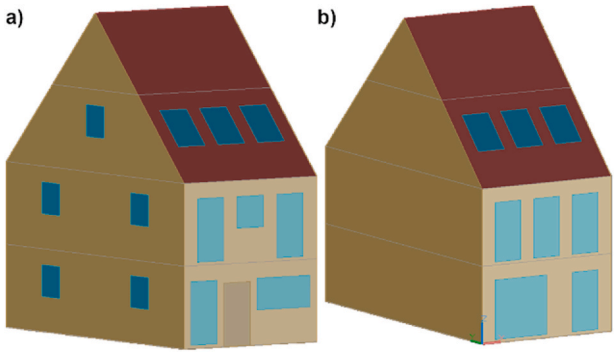

Fig. 2. Schematic depiction of residential building modeled in Energy Plus; a) north and east side, b) south and west side of the building.

3.2. Structure and composition of VO_2:SiO_2 coatings

To investigate the influence of the addition of silica sol on the coating structure and the VO_2 domain size, we performed SEM and surface roughness analysis of all prepared coatings. Furthermore, to investigate a potential relationship between the surface structure and the mechanical robustness, we performed a pencil hardness test to investigate the scratch resistance of the thermochromic coatings. By combining SEM topography information from the Everhart-Thornley-Detector (ETD; Fig. 4) with material information from the Circular Backscatter Detector (CBS; Fig. S5), the surface structure of the coatings could be investigated in detail. We started by analyzing the pure VO_2 coating as reference. Via SEM we observed an incomplete and inhomogeneous surface coverage of the silica coated glass substrate with circular V poor regions, which are surrounded by V rich regions (Figs. 4a and S5a). Here partial dewetting of VO_2 occurred during thermal anneal, which led to a relatively rough surface structure. This inhomogeneous surface coverage

Table 1
Molar ratio and withdrawal speed for preparation of thermochromic coatings with varying VO_2:SiO_2 composition and thickness.

Coating	Coating composition VO_2:SiO_2 [% v/v]	Coating formulation molar ratio VO_2:SiO_2	Withdrawal speed [mm·s^{-1}]	Coating thickness [nm]	Roughness [R_q]
Pure VO_2	100:0	1:0	5	100	0.67
1	40:60	1.5:1	2.5	102	0.56
2a	50:50	2.2:1	1.3	47	0.41
2b	50:50	2.2:1	2	96	0.50
2c	50:50	2.2:1	4	140	1.14
3	70:30	5.1:1	2	96	0.69

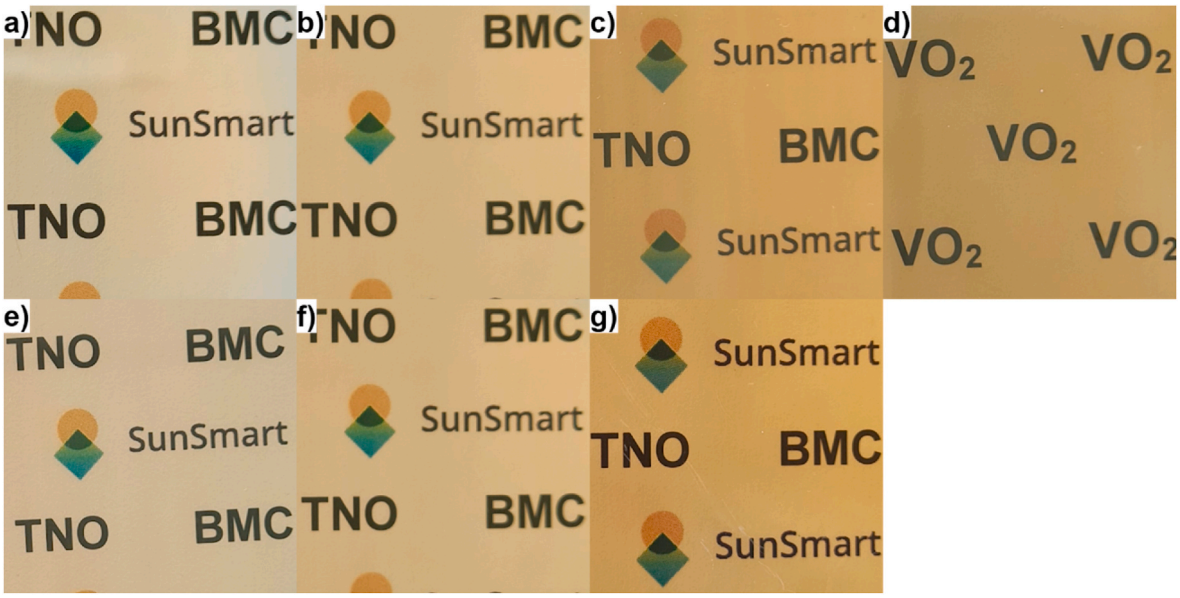

Fig. 3. Thermochromic coatings at layer thickness around 100 nm and varying composition of a) 40% v/v (**1**), b) 50% v/v (**2b**), c) 70% v/v (**3**), d) 100% v/v VO_2, and coatings at 50% v/v VO_2 at varying layer thickness of e) 47 nm (**2a**), f) 96 nm (**2b**), and g) 140 nm (**2c**).

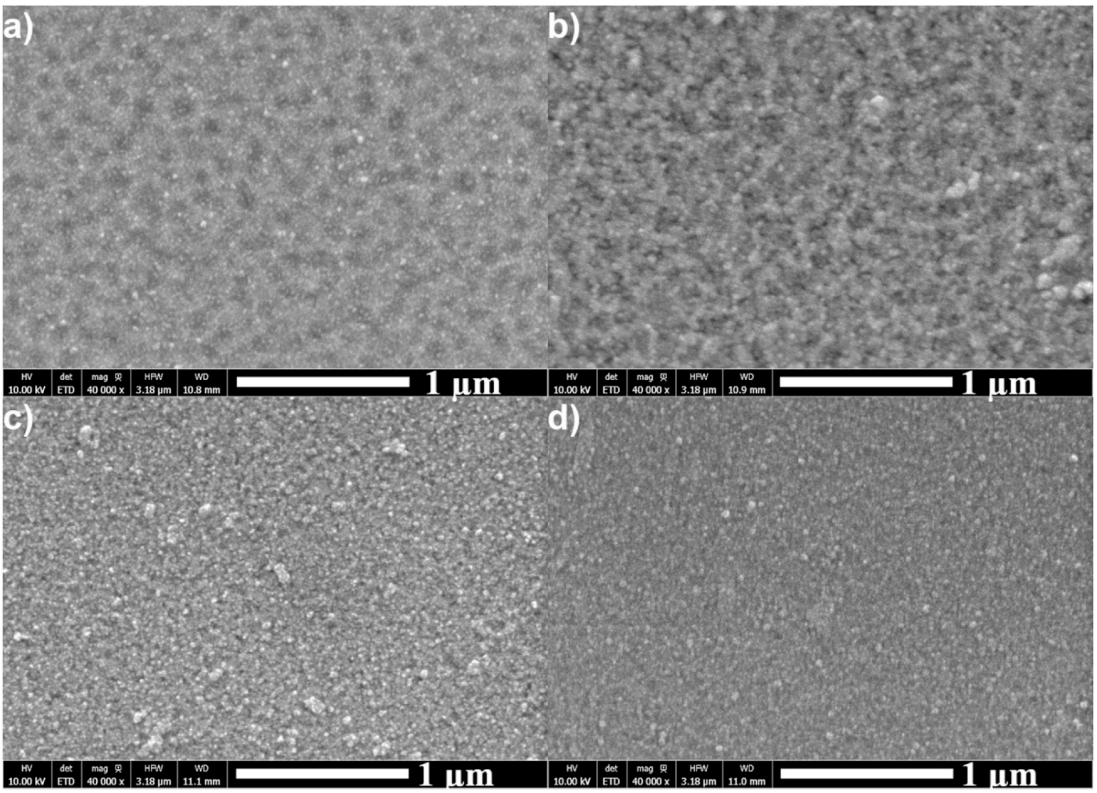

Fig. 4. SEM images of thermochromic coatings at layer thickness around 100 nm and varying composition of a) 100% v/v, b) 70% v/v (**3**), c) 50% v/v (**2b**), d) 40% v/v VO_2 (**1**).

and high surface roughness could be confirmed via optical profilometry measurements resulting in an *Rq* value of 0.67 (Table 1). Furthermore, it is reasonable to assume that this inhomogeneous, rough surface is sensitive to scratching, pollution, etc. This assumption could be confirmed by poor mechanical robustness represented by a pencil hardness $<$ 1H.

By addition of silica to VO_2, we intended to not only improve the optical properties of the thermochromic coating, as discussed in section 3.3, but also to improve the durability of the coating layer. Here the intention was to create a silica matrix, which uniformly covers the substrate and embeds the VO_2 domains in a smooth coating layer. This way the matrix can protect the VO_2 domains against oxidation and the smooth surface structure enables sharp objects to slide over the surface without damaging it, hereby increasing scratch resistance. Analyzing VO_2:SiO_2 coatings **1–3** via SEM, we observed that an increase in silica content led to an increased homogeneity in coating surface structure and V distribution in the coating layer (Fig. 4b–d, S5b-d). For coating **3** with

30% v/v SiO_2 still a relatively inhomogeneous surface structure was visible (Fig. 4b). The addition of SiO_2 led to a slight improvement when compared to the pure VO_2 coating. In coating **3** the de-wetting led to randomly structured and distributed domains with high and low coating thickness. Furthermore, a clear distinction between V rich and poor regions could be observed via back scattering images from the SEM CBS detector (Fig. S5b), showing an inhomogeneous distribution of V in the coating. Coating **3** still showed a similar roughness to the pure VO_2 coating with an *Rq* value of 0.69 (Table 1), but the addition of SiO_2 led to an increase in scratch resistance from < 1H to 4H. Further increase in SiO_2 content in the coating ≥ 50% v/v for coating **1** and **2b** yielded a homogeneous surface structure (Fig. 4c and d). Both coatings showed a relatively smooth surface with no clear distinction between thicker and thinner surface coverage of the substrate by the coating. This indicates a minimum content of SiO_2 in the coating mixture of 50% is needed to enable a smooth surface and homogeneous distribution of the V content in this coating matrix. A relatively homogeneous distribution of V in the coating matrix could be observed for coating **2b** (Fig. S5c), which further improved for coating **1** with 60% v/v SiO_2, where almost no distinction between V rich and poor regions was possible via SEM (Fig. S5d). The homogeneous coating structure coincided with a low surface roughness and resulted in *Rq* values of 0.50 and 0.56 for coating **2b** and **1**, respectively (Table 1). Furthermore, an increased scratch resistance of 6H and 7H was observed for coatings **2b** and **1**, respectively.

Investigating coatings **2a-c** with the same coating composition of 50% v/v VO_2 but different coating thickness of 47, 96 and 140 nm, respectively, led to no clear impact of coating thickness on surface structure and V distribution in the coating matrix. All three coatings showed a similar, relatively homogeneous surface structure and V distribution (Figs. S6 and S7). Nevertheless, an increase in coating thickness from 48 to 96 and 140 nm for coatings **2a-c**, respectively, led to an increase in surface roughness (Table 1) and a decrease in scratch resistance from 7H to 6H and 5H for coatings **2a-c**, respectively. All VO_2:SiO_2 coatings showed a better scratch resistance than sputtered silver coatings which are commonly used in energy-efficient low-e glazing [31].

Due to limitations in magnification, the exact VO_2 domain sizes in the coatings couldn't be analyzed via SEM, and the coating material was therefore further characterized via STEM-EDX (*vide infra*). To investigate if the VO_2 domains form a directional pattern either in the pure VO_2 coating or in the VO_2:SiO_2 coatings, we performed UV–vis–NIR spectrophotometric analysis under a fixed angle with polarized light. Here anisotropy in the coatings should be visible by a change in light transmission for different polarization angles. All composite coatings **1–3**, as well as the pure VO_2 coating, showed no change in light transmission upon change of polarization angle, indicating isotropic optical properties (Fig. S8).

For a more detailed analysis of phase separation between VO_2 and SiO_2 and to investigate the VO_2 domain size and distribution, we performed STEM-EDX analysis of scraped off coating material. We started by analyzing coating **2b** in the three stages of preparation, i.e. as xerogel directly after dip coating, as amorphous material after the first annealing step and as partially crystalline material after the final anneal. Here we observed that within the xerogel stage we still have a homogeneous molecular mixture of VO_2 and SiO_2 without any phase separation (Fig. 5a). After the first annealing step we still see mainly a homogeneous mixture of VO_2 and SiO_2 with small elongated, curled needles on the surface (Fig. 5b–d). After the final anneal we observe that phase separation between VO_2 and SiO_2 has partly occurred with VO_2 mainly forming elongated domains of 100–200 nm in length and 20–50 nm in width (Fig. 5e–h). Here we can conclude that during the anneal process phase separation between VO_2 and SiO_2 starts on the surface of the coating during the first annealing step. In the second annealing step, the VO_2 crystals grow mainly in one direction resulting in elongated crystals of 100–200 nm length embedded in a SiO_2 matrix. Furthermore, we can conclude that not all vanadium species have been converted to crystalline monoclinic VO_2 and that other V-containing species are still partly present, homogeneously mixed in the SiO_2 matrix. Via DSC measurements of scraped off coating material we could show in a previous study that VO_2 (M) was the only crystalline material present in the coating with a degree of purity of approximately 54% with the remaining VO_2 content being amorphous [9].

After investigating the formation of VO_2 domains, we analyzed the impact of VO_2 content in the VO_2:SiO_2 coatings **1–3** on the final VO_2 domain size and distribution. Here we observed that not only the size and distribution but also the shape of the VO_2 domains was influenced by the VO_2 content. Coating **3** with a VO_2 content of 70% v/v showed mostly spherical or ellipsoidal VO_2 domains in a SiO_2 matrix (Fig. 6a).

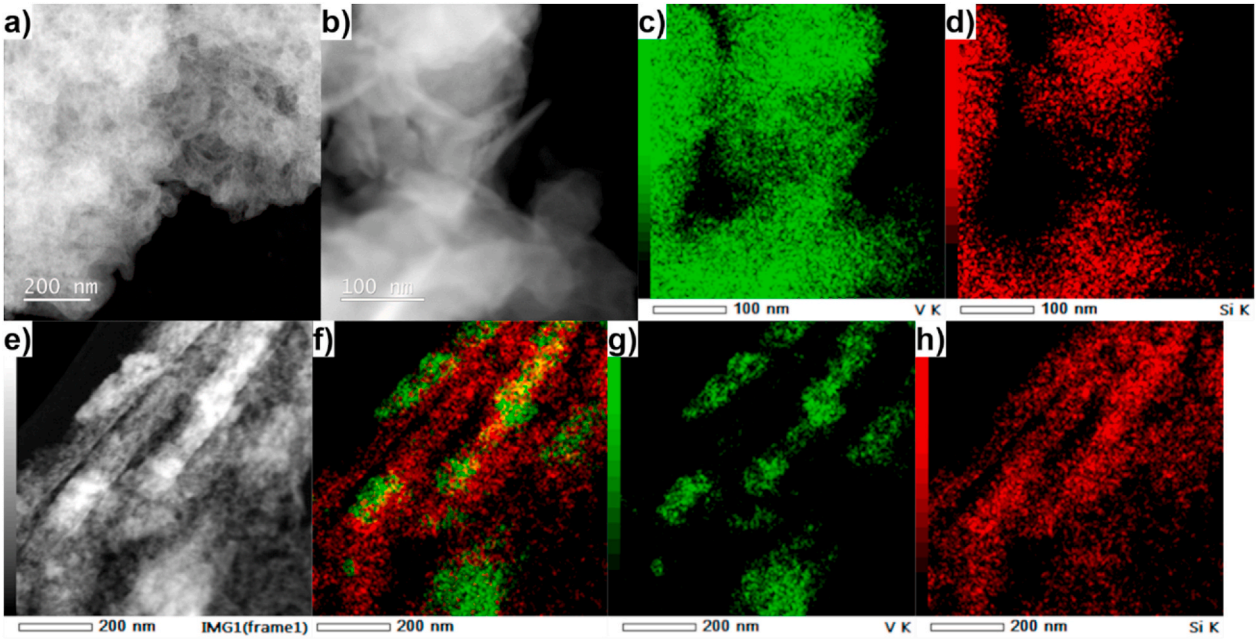

Fig. 5. STEM-EDX analysis of coating **2b** as xerogel after dip coating (a), after the first annealing step (b–d) and in the final state (e–h) (EDX mapping: green = V, red = Si). (For interpretation of the references to color in this figure legend, the reader is referred to the Web version of this article.)

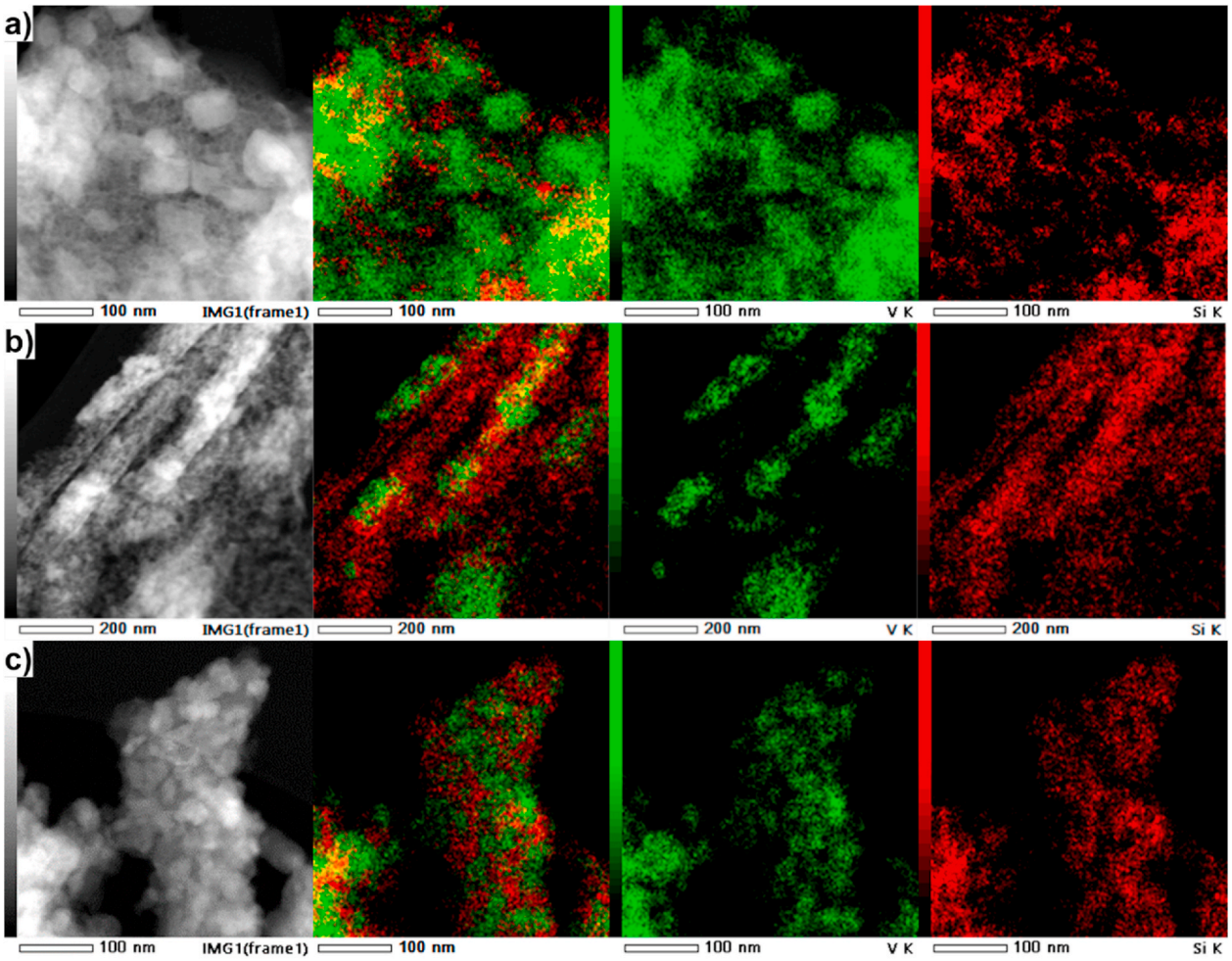

Fig. 6. STEM-EDX analysis of a) coating **3** with 70% v/v VO_2, b) coating **2b** with 50% v/v VO_2 and c) coating **1** with 40% v/v VO_2 (EDX mapping: green = V, red = Si). (For interpretation of the references to color in this figure legend, the reader is referred to the Web version of this article.)

The domains showed a relatively small size distribution with an average diameter of 50 nm. Coating **2b** with a lower VO_2 content of 50% v/v showed mainly rod-shaped VO_2 domains with common lengths between 100 and 200 nm and thicknesses between 20 and 50 nm (Fig. 6b). In general the size distribution increased from coating **3** to **2b**. Coating **1** with the lowest VO_2 content of 40% v/v showed again mostly spherical or ellipsoidal VO_2 domains in a SiO_2 matrix (Fig. 6c). For this coating the VO_2 domains showed an average diameter of 20 nm with a small size distribution. In general it could be observed that the VO_2:SiO_2 ratio has a significant influence on VO_2 domain size and shape, with the smallest domain sizes realized at the lowest VO_2 content.

Furthermore, we analyzed the influence of coating thickness on VO_2 domain size, distribution and morphology in coatings **2a-c** with the same VO_2 content of 50% v/v. Here coating **2a** at 47 nm thickness showed mostly spherical or ellipsoidal VO_2 domains in a SiO_2 matrix (Fig. 7a). The domains showed a relatively small size distribution with an average diameter of 30 nm. Coating **2b** with an increased thickness of 96 nm showed mainly elongated VO_2 domains with common lengths between 100 and 200 nm and thicknesses between 20 and 50 nm (Fig. 7b). For coating **2c** with the largest coating thickness of 140 nm plate like VO_2 crystals were observed with a diameter of several hundred nm (Fig. 7c). As a general trend it was observed that with increasing coating thickness at a VO_2 content of 50% v/v, small spherical particles grow to elongated crystals and finally form plate-like VO_2 domains.

The in-depth STEM-EDX analysis of VO_2:SiO_2 coatings shows that phase separation between V and Si rich regions doesn't occur already after coating application and drying. In the xerogel stage, the vanadium oxalate complex is still highly dispersed in the forming SiO_2 matrix. At temperatures at which the oxalate ligand starts decomposing, first VO_2 crystals are being formed, which further grow during the high temperature crystallization phase. In a 50% v/v VO_2 coating the crystal growth is faster than nucleation of new crystals, which leads to an increased crystal size with increased coating thickness. Here the increased amount of VO_2 leads to a crystal growth from small spheres, to elongated crystals and plate like particles. In a 40% v/v VO_2 coating, the crystal growth is slowed down by the increased dispersion. Here nucleation of new crystals is preferential, which leads to small spherical particles in the SiO_2 matrix. For composite coatings with an increased VO_2 content of 70% v/v, the low amount of SiO_2 is not able to form a complete matrix enabling free mobility of VO_2 during crystallization. Here VO_2 starts to crystallize locally and forms spherical crystals of medium size.

3.3. Influence of composition and coating thickness on thermochromic properties

Schläfer et al. reported optical simulations that predict that with increasing silica content VO_2 coatings at the same ΔT_{sol} values will show increasing T_{vis} [7]. Experimentally, they only provided a proof of concept and prepared coatings with high ΔT_{sol} values up to 16% at T_{vis} values of 46%. Furthermore, they investigated the influence of different silica sources (particles vs. sol). A detailed experimental investigation of the impact of coating thickness and composition on the optical properties was not within the scope of their study. To investigate this, we measured UV–vis–NIR transmission spectra for coatings with a thickness

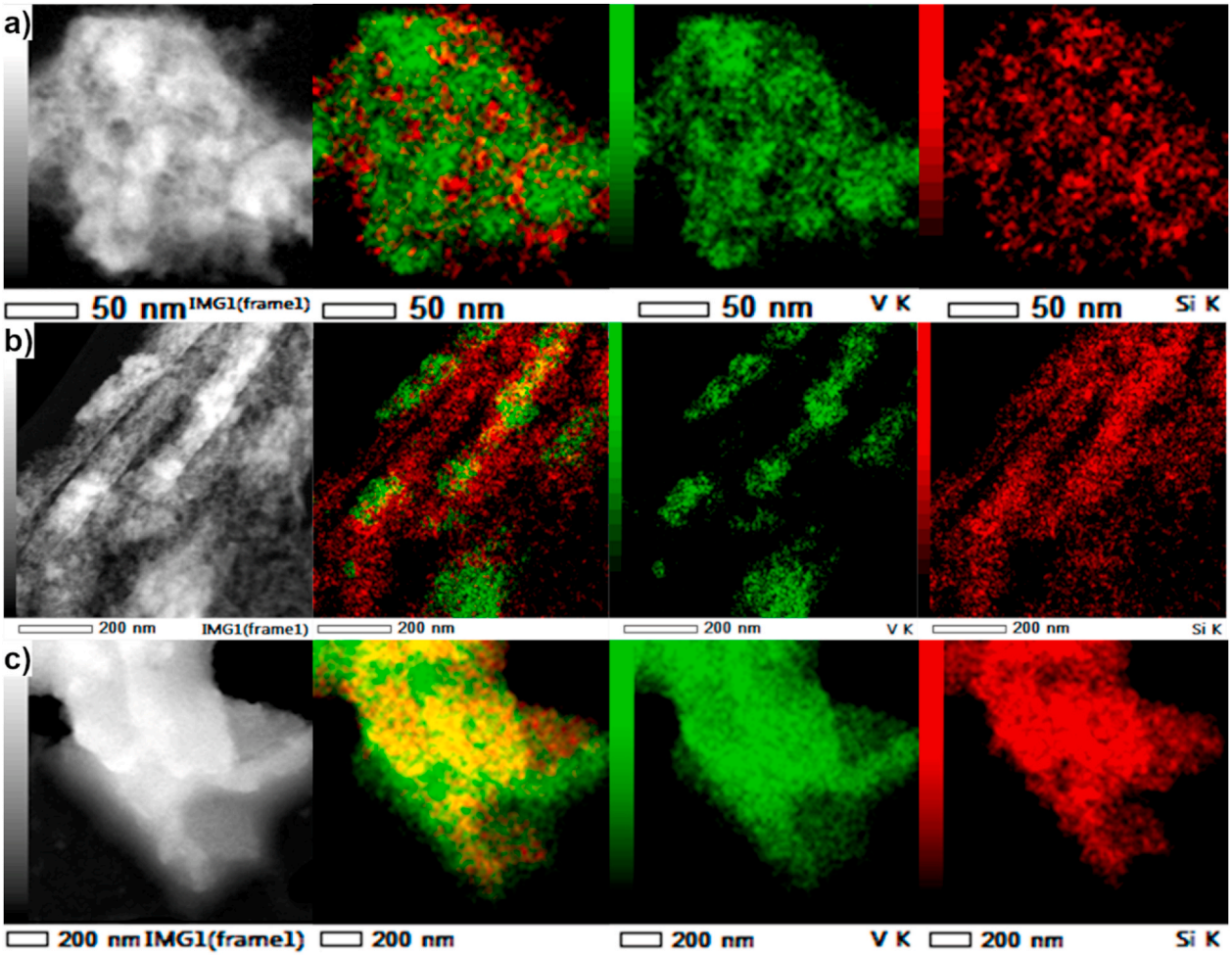

Fig. 7. STEM-EDX analysis of a) 47 nm thick coating **2a**, b) 96 nm thick coating **2b** and c) 140 nm thick coating **2c** (EDX mapping: green = V, red = Si). (For interpretation of the references to color in this figure legend, the reader is referred to the Web version of this article.)

around 100 nm and varying composition. The pure VO_2 coating with a thickness of 100 nm showed a T_{vis} in the cold state of 44% and a ΔT_{sol} of 5.6% (Fig. 8, Table 2). The low solar modulation results partly from the fact that the visible transmission increases to 49% when switching from cold to hot state. This reduces the overall solar modulation and is also not desired in the final application. When 30% v/v of SiO_2 was present in coating **3** with a thickness of 96 nm, the visible transmission slightly increased in the cold state in comparison to pure VO_2 (Fig. 8). Additionally, for the VO_2:SiO_2 coating **3** T_{vis} doesn't change upon phase

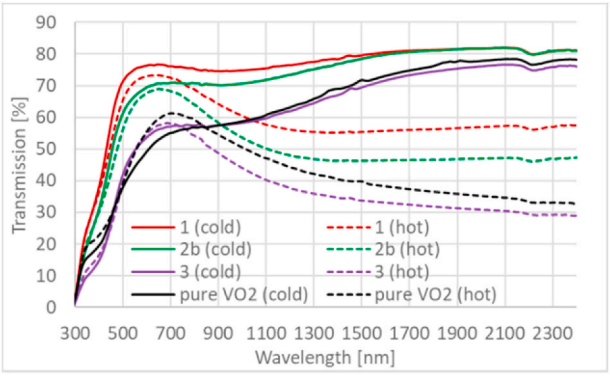

Fig. 8. UV–vis–NIR transmission spectra of VO_2:SiO_2 coatings **1**–**3** with varying compositions and coating thickness around 100 nm and pure VO_2 coating at similar coating thickness as reference.

Table 2
Optical properties of thermochromic coatings with varying VO_2:SiO_2 composition and thickness.

Coating	T_{vis} [%]	ΔT_{sol} [%]	T_{switch} [°C]	Hysteresis width [K]	Hysteresis gradient [K]	T_0 [°C]	ΔT_0 [K]
Pure VO_2	44	5.6	84.8	44.8	6.8	81	30
1	74	10	81.4	36	8.3	78	26
2a	68	8.4	80.1	22.4	10.8	75	13
2b	66	11.8	90.8	28.2	10.9	85	17
2c	61	15.3	88.5	29	11.7	81	14
3	49	10.4	85.6	24.5	10.2	79	11

transition and the IR transmission in the hot state is slightly lower than for pure VO_2. This leads to a large increase in solar modulation in comparison to pure VO_2. Overall the VO_2:SiO_2 coating **3** with 70% v/v VO_2 and a thickness of 96 nm showed a T_{vis} of 49% and a ΔT_{sol} of 10.4% (Table 2). By increasing the silica content further to 50% v/v, the visible transmission could be increased even further. Coating **2b** with a VO_2 content of 50% v/v and a thickness of 96 nm showed a largely increased T_{vis} in the cold state of 66% (Fig. 8, Table 2). Here also the IR transmission in the cold state is increased in comparison to the pure and the 70% v/v VO_2 coating. Additionally, a slight reduction in visible transmission to 63% upon switch from cold to hot state was visible and the IR transmission in the hot state was slightly higher than for pure VO_2. Still a large change in IR transmission occurred which leads to an overall ΔT_{sol}

of 11.8% (Table 2). Another change that was visible with addition of 50% v/v silica was a reduced absorption of violet (380–450 nm) and blue (450–485 nm) light, which resulted in less intense coloration of the coated glass plate (Figs. 3 and 8). Increasing the silica content above 50% v/v led to a further increase in visible transmission and a slight reduction in solar modulation. Coating **1** with a VO_2 content of 40% v/v and a thickness of 102 nm showed a T_{vis} of 74% and a ΔT_{sol} of 10.0% (Fig. 8, Table 2). The coating with the highest silica content showed a similar IR transmission in the cold state as the 50% v/v VO_2 coating **2b**, but a slightly higher IR transmission in the hot state, which ultimately leads to a small reduction in solar modulation. Furthermore, the change in visible transmission upon phase transition increased slightly to ΔT_{vis} = -4%. Overall our results confirm the predictions by Schläfer et al. [7] that an increase in SiO_2 content in VO_2:SiO_2 composite coatings at similar coating thickness increased T_{vis} at a constant ΔT_{sol}.

Since the optical properties of the VO_2:SiO_2 coatings are also dependent on the coating thickness, we investigated the thermochromic properties of coatings with 50% v/v VO_2 and thicknesses between 48 and 140 nm. The VO_2:SiO_2 coating **2a** with a thickness of 48 nm showed a high visible transmission of 68% in the cold as well as in the hot state (Fig. 9, Table 2). The change in transmission upon switch occurred exclusively in the IR region with a total solar modulation of 8.4% (Table 2). When doubling the coating thickness a slight decrease in visible transmission was observed and coincided with a significant increase in solar modulation. Coating **2b** with a thickness of 96 nm showed a T_{vis} of 66% and a ΔT_{sol} of 11.8% (Fig. 9, Table 2). The change in IR transmission upon switch increased significantly in comparison to the thinner coating **2a**. Additionally, a slight reduction in T_{vis} during phase transition was visible, which in combination led to the large increase in solar modulation. Further increase in coating thickness again led to a small reduction in visible transmission and a large increase in solar modulation. The VO_2:SiO_2 coating **2c** with a thickness of 140 nm still showed a high T_{vis} in the cold state of 61%, which is only a reduction of 5% in comparison to coating **2b** (Fig. 9, Table 2). But **2c** showed an increased change in visible transmission upon switch to ΔT_{vis} of -5%. In combination with only a slight decrease in IR transmission in the cold state but a signification decrease in the hot state in comparison to **2b**, this led to a large increase in ΔT_{sol} to 15% (Fig. 9, Table 2). The coating **2c** showed the highest solar modulation of all coatings prepared in this study. Overall the results show that for increasing coating thickness at constant coating composition a large increase in ΔT_{sol} can be achieved with only slightly reducing T_{vis}, which can have significant impact on the potential for application in energy-efficient glazing.

For application of VO_2 coatings in energy-efficient windows it is important to combine high T_{vis} with high ΔT_{sol} values. For all 6 categories of thermochromic VO_2 coatings and films mentioned in the introduction we selected 5 reported coatings/films with the highest combination of T_{vis} and ΔT_{sol} and compared them to the coatings reported in this study (Fig. 10). It can be seen that especially coatings **1**, **2b** and **2c** exceed almost all other reported high performing VO_2 coatings and are similar in performance to nanocomposite films. The few VO_2 coatings with comparable performance are either not commercially feasible, due to the use of hydrothermal growth of coatings on glass [14], freeze drying [15] or the use of complex (hollow) core shell particles [16,17], or combine high solar modulation with a low visible transmission of T_{vis} < 55% [20–23]. In this comparison, we can show that with our VO_2:SiO_2 coatings we have reached the performance of nanocomposite films at T_{vis} values > 60%. For application purposes these coatings show high potential as coated glass in energy-efficient windows, whereas nanocomposite films are suited for laminated glass only.

The very good performance of the VO_2:SiO_2 coatings in this study can be explained by the distribution of VO_2 in a dielectric medium and by the purity and crystallinity of the functional VO_2 in the coatings. A measure for purity and crystallinity of VO_2 is the transition enthalpy in J g^{-1}. To analyze the VO_2 domains in our composite coatings, we used data of DSC measurements of scraped off coating material that we reported previously [9]. Here the thermodynamic switching temperature (T_0) for the VO_2 (M) → VO_2 (R) and VO_2 (R) → VO_2 (M) phase transition was 72 °C and 62 °C, respectively. The switching enthalpy of the analyzed coating material, consisting of 50% v/v VO_2, was 22.3 J g^{-1} corresponding to a degree of purity of the crystalline VO_2 (M) phase of approx. 54%.

To investigate the influence of silica content and coating thickness on the phase transition, we measured temperature dependent transmission spectra of all 5 VO_2:SiO_2 coatings and the pure VO_2 coating as reference. The coated glass plates were heated up in small temperature steps to above the switching temperature and were subsequently slowly cooled down. Hysteresis plots were prepared for all coatings and the hysteresis width and gradient were analyzed (Fig. 11a and b, Figs. S9–S13, Table 2). The pure VO_2 coating showed a switching temperature (T_{switch}) from cold to hot state at 84.4 °C and a very broad hysteresis width of 44.8 K with a small gradient upon heating of 6.8 K (Fig. S9, Table 2). The thermodynamic switching temperature (T_0) for the pure VO_2 coatings was at 81 °C for the insulator to metal transition (IMT), with a difference (ΔT_0) between T_0 for IMT and metal insulator transition (MIT) of 30 K. The high T_{switch} and broad hysteresis width are due to the structure of the pure VO_2 coating, which consists of inhomogeneous VO_2 clusters of various sizes and an inhomogeneous coverage of the substrate (Fig. 4a). Addition of 30% v/v of silica in coating **3** led to a significant reduction in hysteresis width to 24.5 K and only a minor increase in transition gradient to 10.2 K (Fig. S10, Table 2). Here the silica matrix led to a more homogeneous surface coverage and decreased size distribution of VO_2 domains (Fig. 4b). Furthermore, it was observed that the average

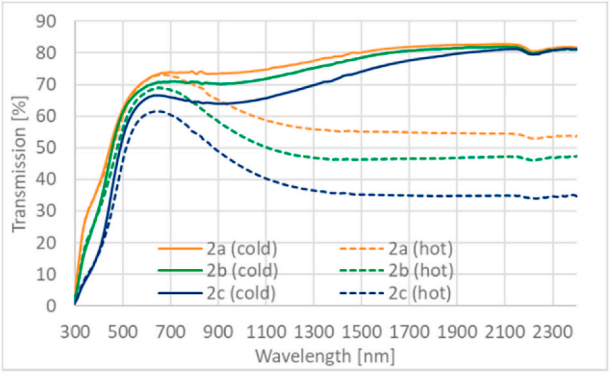

Fig. 9. UV–vis–NIR transmission spectra of VO_2:SiO_2 coatings **2a-c** with 50% v/v VO_2 and varying coating thickness.

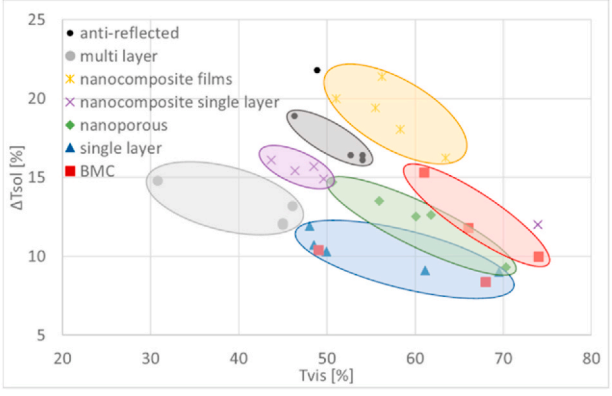

Fig. 10. Performance comparison between best performing thermochromic coatings/films and our reported VO_2:SiO_2 coatings (red squares). (For interpretation of the references to color in this figure legend, the reader is referred to the Web version of this article.)

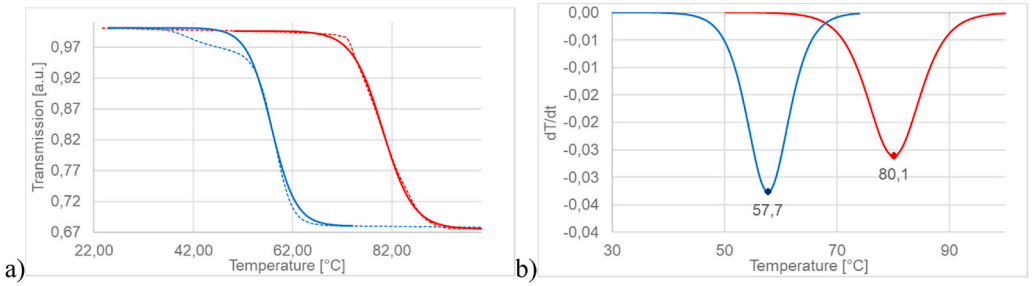

Fig. 11. a) Measured (dotted) and fitted (full line) relative transmission at 1600 nm of VO_2:SiO_2 coating **2a** as function of temperature upon heating (red) and cooling (blue). b) First derivative of hysteresis plot with indication of T_{switch}, hysteresis width and gradient. (For interpretation of the references to color in this figure legend, the reader is referred to the Web version of this article.)

VO_2 domain size was reduced to 50 nm (Fig. 6a). The smaller domain size and therefore larger surface area, coinciding with a small size distribution, leads to a narrowing of the hysteresis width. T_{switch} was not impacted by addition of 30% v/v silica, whereas T_0 was slightly reduced to 78 °C and ΔT_0 was reduced to 11 K. Further increase in silica content with similar coating thickness led to an increase in hysteresis width to 28.2 K and 36.0 K for coatings **2b** and **1**, respectively, without significant change in hysteresis gradient (Figs. S11 and S12, Table 2). It was observed that for coating **2b** the VO_2 domains had a rod-like shape with a length between 100 and 200 nm and a width between 20 and 50 nm (Fig. 6b). Additionally, the size distribution increased slightly. The changes in VO_2 domain size, size distribution and shape negatively influence the hysteresis gradient. For coating **1**, spherical VO_2 domains with an average diameter of 20 nm and a small size distribution were observed (Fig. 6c). No clear trend for the change in T_{switch} was observed since it first increased to 90.8 °C for coating **2b** with 50% v/v silica and then was reduced significantly to 81.4 °C for coating **1** with 60% v/v silica. The same observation was made for T_0, which was increased to 85 °C for coating **2b** and reduced to 78 °C for coating **1**. Furthermore, ΔT_0 increased with increasing silica content to 17 and 26 K for coating **2a** and **1**, respectively. Via the thermodynamic switching temperature values, it can be concluded that for spherical VO_2 domains a reduction in domain size leads to a reduction in switching temperature. The increased surface to volume ratio is likely to increase the number of surface defects and therefore the nucleation sites for the phase transition [32]. Here the deviation of coating **2b** can be explained by the change in VO_2 domain geometry from spherical to elongated. Investigating the influence of coating thickness on the transition temperature, as well as on the hysteresis gradient and width, we observed that at thicknesses >100 nm no major change occurred (Fig. S13, Table 2). T_{switch}, T_0 and ΔT_0 were slightly reduced and transition hysteresis and gradient were slightly increased by increasing the coating thickness from 96 to 140 nm at constant VO_2 content for coatings **2b** and **c**, respectively. The coating **2c** with a thickness of 140 nm showed plate-like VO_2 domains with average diameters of several hundred nm (Fig. 7c). Here the structure of the VO_2 domains has a similar impact on the phase transition as for coating **2b** with elongated crystals. Only very thin coatings of 48 nm showed a slightly lower hysteresis width of 22.4 K and a significantly lower T_{switch} and T_0 of 80.1 and 75 °C, respectively (Fig. 11, Table 2). For coating **2a**, small spherical VO_2 domains with average diameter of 30 nm and a small size distribution were observed (Fig. 7a). The similar size and shape of VO_2 domains for coating **1** and coating **2a** at different coating thickness and composition resulted in similar T_{switch}, T_0 and hysteresis gradient values. Therefore we can conclude that the IMT is mainly influenced by the VO_2 domain size and shape. ΔT_0 and transition hysteresis deviated significantly, since the MIT for the higher diluted coating **1** started at a much lower T_0. Here the matrix shows a significant impact on the phase transition from rutile to monoclinic, which increases the difference in T_0 between IMT and MIT. In general it can be concluded that the VO_2 domain size and shape, as well as the matrix can have a major influence on the switching behavior. Small, spherical VO_2 domains with a small size distribution lead to a low IMT temperature and a small hysteresis gradient. Overall introducing VO_2 domains in a silica matrix increases the transition temperature for the MIT and reduces the hysteresis width. Here, increased dilution slightly reduces the MIT temperature and increases the hysteresis width.

3.4. Long-term stability of VO_2:SiO_2 coatings

To select relevant durability and lifetime tests for VO_2:SiO_2 coatings, we have to consider where the coating will be placed in the final application as a smart window and what kind of conditions the coating is exposed to during production and use of an IGU. Coatings for energy-efficient glazing are usually applied on side 2 (Fig. 1) of an IGU. In that position they show the best performance in reducing solar or radiator heat transmission, and are also shielded from the outside environment and therefore better protected against degradation. For thermochromic coatings the positioning on side 2 has an additional importance, since the switch of the material has to be based on the temperature of the exterior glass pane. The atmosphere in the gap of high performance IGUs commonly consists of argon, which means that the coating is not in contact with oxygen. The only requirement for an energy-efficient coating placed on side 2 of an IGU is to withstand UV radiation according to EN 1096-3 [33]. To analyze UV stability similar to EN 1096-3, we exposed a coated glass plate with a 60 nm thick VO_2:SiO_2 coating with 70% v/v VO_2 to UV radiation for more than 1000 h. All testing conditions, such as setup and UV source, were set to comply with the definitions in the standard taking into account limitations due to sample size. To analyze potential degradation, we measured UV–vis–NIR spectroscopy before and after 139, 726 and 1220 h exposure to UV radiation (Fig. S14). No change in optical properties in the hot and the cold state could be observed over the whole testing period. Therefore, we can conclude that the coating withstands UV radiation according to EN 1096-3 and passes the critical requirements for energy-efficient coatings in windows.

Since the coating is protected in the final application within an IGU with argon atmosphere, UV stability is the only relevant stability criterium for the thermochromic coating in the finished smart window. Nevertheless, after coating application until assembly of the IGU several months can pass, where the coating will be subjected to standard air atmosphere. Therefore, it is important for the industrial processing of the coated glass that it can withstand several months in contact with air under standard conditions (20 °C, 40% humidity) without deterioration of the optical properties. To investigate the degradation behavior of the VO_2:SiO_2 coatings in air we exposed a coated glass plate with a 50 nm thick coating with 70% v/v VO_2 to the standard environment in our lab of 20 °C and 40% humidity and measured UV–vis–NIR spectroscopy for a duration of 11 months. Within this period no deterioration of the optical properties was observed in the hot and the cold state (Fig. S15). Therefore it can be concluded that the stability of the VO_2:SiO_2 coatings is sufficient for industrial processing into IGUs.

3.5. Energy savings potential of VO_2:SiO_2 coatings

To evaluate the energy savings potential of the high performance VO_2:SiO_2 coatings, we performed building energy simulations. Here we designed a typical Dutch building and used Beek as a location for the simulations. Since > 60% of Dutch residential buildings are either duplex or terraced houses [34], we selected a building with one side without contact to the outside environment. Furthermore, we designed wall insulation to reach an *Rc* value (thermal resistance of the composite) of 4.7 m^2 K W^{-1}, in agreement with current Dutch regulations. Additionally, we selected a size of 130 m^2 living space and 35 m^2 of windows, which are common values for a 4 person household in the Netherlands (Figs. 2 and S1). In the simulation we used VO_2:SiO_2 coatings **1**, **2b** and **2c**, which show the highest combination of T_{vis} and ΔT_{sol}, in a double glazing unit combined with a standard low-e coating. The annual energy consumption for a building equipped with either one of these three smart windows or a low-e glazing was compared to clear double glazing to calculate annual energy and cost savings (Fig. 12). With these simulations we could show that all three analyzed smart windows can significantly reduce annual energy consumption and lead to energy savings between 23 and 24%, which is a relative improvement of 10% over low-e glazing. The smart window with VO_2:SiO_2 coating **1** shows the highest energy savings of 23.8%. Here the high T_{vis} of 66% with a cold state *G* value of 0.52 and a *U* value of 1.0 W m^{-2} K^{-1} of the smart window, leads to a reduction of annual heating demand of 16.4%, which is the highest energy savings for heating of all analyzed smart windows. Since heating demand for the simulated building in Beek equals > 70% of the total energy costs, the window with the highest energy savings for heating has also the highest impact on total energy savings. The smart windows with VO_2:SiO_2 coatings **2b** and **2c** show even higher reduction in annual cooling demand with up to 71% savings due to hot state *G* values of 0.46 and 0.41, respectively. But due to lower energy savings for heating of 14.0% and 10.2%, respectively, the overall energy savings are with 23.7% and 23% lower than for the smart window with coating **1**. Taking into account the average cost price for electricity and gas in the Netherlands the annual cost savings for the three smart windows can be calculated [35]. Here an individual household can save up to 470 € per year in comparison to the use of double clear glass.

4. Conclusions

In conclusion, we developed an industrially applicable procedure to synthesize high performance thermochromic coatings on glass via liquid coating deposition with subsequent thermal curing. The combination of VO_2 and SiO_2 in a composite coating made from sol-gel mixtures leads to small homogeneously distributed VO_2 domains in a silica matrix. During thermal anneal of the xerocoat, phase separation yielding V rich and Si rich regions occurs. We investigated this phase separation in detail and concluded that the crystal growth is dependent on the composition (V:Si ratio) and thickness. Due to the high crystallinity and small particle size of the VO_2 domains in the SiO_2 matrix unrivalled optical properties are achieved. The combination of T_{vis} > 60% and $\Delta T_{sol} \geq$ 10% of the composite coatings is exceeding comparable coatings reported to date, and makes these coatings suitable for application in smart windows. We showed that the balance between T_{vis} and ΔT_{sol} can be influenced by the VO_2:SiO_2 ratio and the coating thickness, enabling the customization of optical properties for different climate zones or building types for optimum energy savings. The different VO_2 domain sizes and shapes and the silica matrix have a major impact on the phase transition. We demonstrated that small, spherical VO_2 domains at a low dilution in a silica matrix lead to optimized transition temperature and hysteresis gradient and width. The silica matrix additionally leads to a smooth coating surface and encapsulates the VO_2 domains. This leads to an increased stability of the composite coatings in comparison to pure VO_2 coatings. Here we demonstrated that the composite coatings withstand stability tests relevant for energy-efficient coatings in IGUs. Additionally, we showed that with a scratch resistance $\geq$ 4H and a stability in ambient environment of at least 11 months, the coatings are suitable for industrial processing into IGUs. With building energy simulations on a typical Dutch building, we demonstrated that the use of smart windows with our thermochromic coatings can lead to energy savings of 24%, which equals to annual cost savings of up to 470 € per household.

Funding sources

The research work reported in this paper was carried out within Brightlands Materials Center, a joint research initiative between TNO and the province of Limburg (Netherlands). The work is funded by the Dutch government and the province of Limburg. Additionally, the parts of the work were performed within the OPZuid project LEEF, the Interreg Vlaanderen-Nederland project EnEf and the SIA RAAK Pro project Window of the Future.

CRediT authorship contribution statement

Cindy P.K. Yeung: Validation, Formal analysis, Investigation, Visualization. **Roberto Habets:** Validation, Investigation. **Luc**

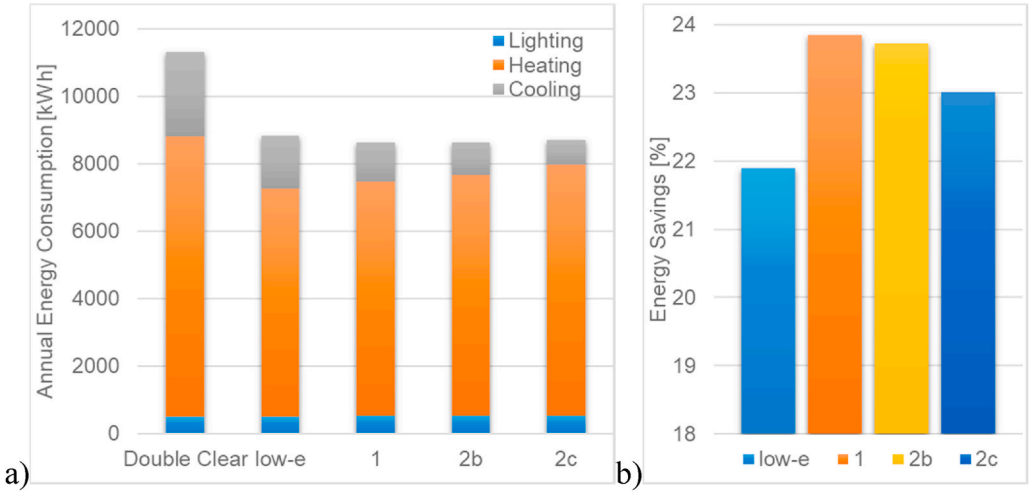

Fig. 12. a) Annual energy consumption of simulated residential building equipped with clear double glazing, low-e glazing or one of the three smart windows and b) annual energy savings of the smart windows over double clear glass and energy savings of low-e glazing as comparison.

Leufkens: Validation, Investigation, Visualization. **Fallon Colberts:** Validation, Investigation. **Kathleen Stout:** Conceptualization, Validation. **Marcel Verheijen:** Investigation, Visualization. **Zeger Vroon:** Conceptualization, Validation. **Daniel Mann:** Conceptualization, Methodology, Validation, Writing – original draft, Writing – review & editing, Visualization. **Pascal Buskens:** Conceptualization, Writing – review & editing, Supervision.

Declaration of competing interest

The authors declare that they have no known competing financial interests or personal relationships that could have appeared to influence the work reported in this paper.

Acknowledgements

We would like to thank Carlo Manders from Eurofins Materials Science for performing the SEM analysis in this study and we would like to acknowledge Solliance for funding the TEM facilities at Eurofins used in this study.

Appendix A. Supplementary data

Supplementary data to this article can be found online at https://doi.org/10.1016/j.solmat.2021.111238.

References

[1] C.G. Granqvist, G.A. Niklasson, Solar energy materials for thermal applications: a primer, Sol. Energy Mater. Sol. Cells 180 (2018) 213–226.
[2] S. Garshasbi, M. Santamouris, Using advanced thermochromic technologies in the built environment: recent development and potential to decrease the energy consumption and fight urban overheating, Sol. Energy Mater. Sol. Cells 191 (2019) 21–32.
[3] Y. Cui, Y. Ke, C. Liu, Z. Chen, N. Wang, L. Zhang, Y. Zhou, S. Wang, Y. Gao, Y. Long, Thermochromic VO2 for energy-efficient smart windows, Joule 2 (2018) 1707–1746.
[4] N. Peys, P. Adriaensens, S. Van Doorslaer, S. Gielis, E. Peeters, Ch De Dobbelaere, S. De Gendt, A. Hardy, M.K. Van Bael, Aqueous citrato-oxovanadate(IV) precursor solutions for VO2: synthesis, spectroscopic investigation and thermal analysis, Dalton Trans. 43 (2014) 12614–12623.
[5] N. Peys, S. Maurelli, G. Reekmans, P. Adriaensens, S. De Gendt, A. Hardy, S. Van Doorslaer, M.K. Van Bael, Chemical composition of an aqueous oxalato-/citrato-VO^{2+} solution as determinant for vanadium oxide phase formation, Inorg. Chem. 54 (2015) 69–78.
[6] Z. Zhang, Y. Gao, Z. Chen, J. Du, C. Cao, L. Kang, H. Luo, Thermochromic VO2 thin films: solution-based processing, improved optical properties, and lowered phase transformation temperature, Langmuir 26 (2010) 10738–10744.
[7] J. Schläefer, C. Sol, T. Li, D. Malarde, M. Portnoi, T.J. Macdonald, S.K. Laney, M. J. Powell, I. Top, I.P. Parkin, I. Papakonstantinou, Thermochromic VO2 - SiO2 nanocomposite smart window coatings with narrow phase transition hysteresis and transition gradient width, Sol. Energy Mater. Sol. Cells 200 (2019) 109944.
[8] J. Zhang, H. He, Y. Xie, B. Pan, Theoretical study on the tungsten-induced reduction of transition temperature and the degradation of optical properties for VO2, J. Chem. Phys. 138 (2013) 114705.
[9] L. Calvi, L. Leufkens, C.P.K. Yeung, R. Habets, D. Mann, K. Elen, A. Hardy, M. K. Van Bael, P. Buskens, A comparison study on the switching kinetics of W/VO2 powders and VO2 coatings and their implications for thermochromic glazing, Sol. Energy Mater. Sol. Cells 224 (2021) 110977.
[10] N. Wang, N.T.C. Shun, M. Duchamp, R.E. Dunin-Borkowski, Z. Li, Y. Long, Effect of lanthanum doping on modulating thermochromic properties of VO2 thin films, RSC Adv. 6 (2016) 48455–48461.
[11] Y.-H. Jung, S.P. Pack, S. Chung, Solvothermal synthesis and characterization of highly monodisperse organically functionalized vanadium oxide nanocrystals for thermochromic applications, Mater. Res. Bull. 101 (2018) 67–72.
[12] N.R. Mlyuka, G.A. Niklasson, C.G. Granqvist, Thermochromic multilayer films of VO2 and TiO2 with enhanced transmittance, Sol. Energy Mater. Sol. Cells 93 (2009) 1685–1687.
[13] N.R. Mlyuka, G.A. Niklasson, C.G. Granqvist, Thermochromic VO2-based multilayer films with enhanced luminous transmittance and solar modulation, Phys. Status Solidi A 206 (2009) 2155–2160.
[14] J. Zhang, J. Li, P. Chen, F. Rehman, Y. Jiang, M. Cao, Y. Zhao, H. Jin, Hydrothermal growth of VO2 nanoplate thermochromic films on glass with high visible transmittance, Sci. Rep. 6 (2016) 27898.
[15] X. Cao, N. Wang, J.Y. Law, S.C.J. Loo, S. Magdassi, Y. Long, Nanoporous thermochromic VO2 (M) thin films: controlled porosity, largely enhanced luminous transmittance and solar modulating ability, Langmuir 30 (2014) 1710–1715.
[16] Z. Qu, L. Yao, J. Li, J. He, J. Mi, S. Ma, S. Tang, L. Feng, Bifunctional template-induced VO2@SiO2 dual-shelled hollow nanosphere-based coatings for smart windows, ACS Appl. Mater. Interfaces 11 (2019) 15960–15968.
[17] L. Yao, Z. Qu, Z. Pang, J. Li, S. Tang, J. He, L. Feng, Three-layered hollow nanospheres based coatings with ultrahigh-performance of energy-saving, antireflection, and self-cleaning for smart windows, Small 14 (2018) 1801661.
[18] L. Zhao, L. Miao, C. Liu, C. Li, T. Asaka, Y. Kang, Y. Iwamoto, S. Tanemura, H. Gu, H. Su, Solution-processed VO2-SiO2 composite films with simultaneously enhanced luminous transmittance, solar modulation ability and anti-oxidation property, Sci. Rep. 4 (2014) 700.
[19] K. Li, M. Li, C. Xu, Y. Luo, G. Li, VO2(M) nanoparticles with controllable phase transition and high nanothermochromic performance, J. Alloys Compd. 816 (2020) 152655.
[20] C. Liu, S. Wang, Y. Zhou, H. Yang, Q. Lu, D. Mandler, S. Magdassi, C.Y. Tay, Y. Long, Index-tunable anti-reflection coatings: maximizing solar modulation ability for vanadium dioxide-based smart thermochromic glazing, J. Alloys Compd. 731 (2018) 1197–1207.
[21] T. Chang, X. Cao, L.R. Dedon, S. Long, A. Huang, Z. Shao, N. Li, H. Luo, P. Jin, Optical design and stability study for ultrahigh-performance and long-lived vanadium dioxide-based thermochromic coatings, Nano Energy 44 (2018) 256–264.
[22] L. Yao, Z. Qu, R. Sun, Z. Pang, Y. Wang, B. Jin, J. He, Long-Lived multilayer coatings for smart windows: integration of energy-saving, antifogging, and self-healing functions, ACS Appl. Energy Mater. 2 (2019) 7467–7473.
[23] C. Sol, M. Portnoi, T. Li, K.L. Gurunatha, J. Schläfer, S. Guldin, I.P. Parkin, I. Papakonstantinou, High-performance planar thin film thermochromic window via dynamic optical impedance matching, ACS Appl. Mater. Interfaces 12 (2020) 8140–8145.
[24] Z. Chen, Y. Gao, L. Kang, C. Cao, S. Chen, H. Luo, Fine crystalline VO2 nanoparticles: synthesis, abnormal phase transition temperatures and excellent optical properties of a derived VO2 nanocomposite foil, J. Mater. Chem. A 2 (2014) 2718–2727.
[25] J. Zhu, A. Huang, H. Ma, Y. Ma, K. Tong, S. Ji, S. Bao, X. Cao, P. Jin, Composite film of vanadium dioxide nanoparticles and ionic liquid-nickelchlorine complexes with excellent visible thermochromic performance, ACS Appl. Mater. Interfaces 8 (2016) 29742–29748.
[26] D. Wang, D. Guo, Z. Zhao, C. Ling, J. Li, S. Hong, Y. Zhao, H. Jin, Surface modification-assisted solvent annealing to prepare high quality M-phase VO2 nanocrystals for flexible thermochromic films, Sol. Energy Mater. Sol. Cells 200 (2019) 110031.
[27] J. Zhu, Y. Zhou, B. Wang, J. Zheng, S. Ji, H. Yao, H. Luo, P. Jin, Vanadium dioxide nanoparticle-based thermochromic smart coating: high luminous transmittance, excellent solar regulation efficiency and near room temperature phase transition, ACS Appl. Mater. Interfaces 7 (2015) 27796–27803.
[28] M.E.A. Warwick, I. Ridley, R. Binions, The effect of variation in the transition hysteresis width and gradient in thermochromic glazing systems, Sol. Energy Mater. Sol. Cells 140 (2015) 253–265.
[29] Energy Plus Building Energy Simulation Software, US Department of Energy. Available online: https://energyplus.net/ (accessed on 01 October 2020).
[30] D. Mann, C. Yeung, R. Habets, Z. Vroon, P. Buskens, Comparative building energy simulation study of static and thermochromically adaptive energy-efficient glazing in various climate regions, Energies 13 (2020) 2842.
[31] E. Ando, S. Suzuki, N. Aomine, M. Miyazaki, M. Tada, Sputtered silver-based low-emissivity coatings with high moisture durability, Vacuum 59 (2000) 792–799.
[32] R. Lopez, T.E. Haynes, L.A. Boatner, Size effect in the structural phase transition of VO2 nanoparticles, Phys. Rev. B 65 (2002) 224113.
[33] European Standard EN 1096-3. *Glass in Building - Coated Glass - Part 3: Requirements and Test Methods for Class C and D Coatings*, Comite Europeen de Normalisation, Brussels, Belgium, 2012.
[34] Netherlands' Housing Survey (WoON); Statistics Netherlands (CBS), The Hague, The Netherlands. https://www.cbs.nl/nl-nl/nieuws/2016/14/vier-op-de-tien-huishoudens-wonen-in-een-rijtjeshuis, 2015. (Accessed 1 October 2020) accessed on.
[35] Energieprijzen, The Netherlands enterprise agency (RVO): the Hague, The Netherlands. https://energiecijfers.databank.nl/dashboard/dashboard/, 2020. (Accessed 1 October 2020) accessed on.